Defect structure of ferromagnetic superconducting RuSr$_2$GdCu$_2$O$_8$

O. I. Lebedev* and G. Van Tendeloo

EMAT, University of Antwerp, Groenenborgerlaan 171, B-2020 Antwerpen, Belgium

J. P. Attfield

Centre for Science at Extreme Conditions, University of Edinburgh, Erskine Williamson Building, King's Buildings, Mayfield Road, Edinburgh EH9 3JZ, United Kingdom

A. C. Mclaughlin

Department of Chemistry, University of Aberdeen, Meston Walk, Aberdeen AB24 3UE, United Kingdom

The structure and defect structure of superconducting ferromagnetic bulk RuSr$_2$GdCu$_2$O$_8$ has been investigated using high-resolution transmission electron microscopy and high-resolution scanning transmission microscopy. Two distinct, but closely related structures, due to ordering of rotated RuO$_6$ octahedra and due to Cu substitution in the Ru-O layer, have been revealed. The structure of Ru$_{1-x}$Sr$_2$GdCu$_{2+x}$O$_{8-\delta}$ can be described as a periodic alteration along the c axis of CuO$_4$ planes and RuO$_6$ octahedra. The unit-cell parameters of this phase are $\sqrt{2}a_p \times \sqrt{2}a_p \times 2c$. The possible influence of this phase and defect structure on the sensitivity of the superconductivity and magnetic properties is discussed. Local defects such as 90° domain boundaries, (130) antiphase boundaries, and the associated dislocations are analyzed.

I. INTRODUCTION

It is difficult to overestimate the importance or the influence of defects or grain boundaries on the physical properties of a material. Local changes in the atomic structure or composition may drastically alter the properties of a material. High-T_C superconducting materials are no exception in this matter and confirm the close correlation of defect structure (interfaces or grain boundaries) and material properties.[1,2] Moreover, the appearance of periodic defects in an existing material can lead to a new phase with different properties. In the Y-Ba-Cu-O system, two phases were first discovered as intergrowths by means of transmission electron microscopy (TEM): YBa$_2$Cu$_4$O$_8$, $T_C \approx 80$ K, and Y$_2$Ba$_4$Cu$_7$O$_{15+x}$, $T_C \approx 40$ K.[3,4] Later they were synthesized as single-phase materials.[4] Also in the Hg-Ba-Ca-Cu-O system the 2212 phase was first detected as a defect in the 1212 phase.[5]

The discovery of the coexistence of superconductivity (SC) ($T_C \approx 48$ K) with ferromagnetic (FM) ordering of the Ru moments ($T_m \approx 132$ K) in the 1212 layered cuprate[6] RuSr$_2$GdCu$_2$O$_8$ is still controversial and requires a very careful structure analysis. Neutron diffraction studies[7,8] also demonstrated an antiferromagnetic (AFM) nature of the Ru moments forming a G-type antiferromagnetic structure. Moreover, there is the antagonistic nature of superconducting and antiferromagnetic ordering suggested by the early paper of Ginzburg.[9]

Several research groups report the coexistence of SC and FM in the ruthenocuprates[10,11] as well as a tuning of the properties by doping.[12,13,7] It was shown that SC can coexist with a FM phase assuming an inhomogeneous structure (crystalline, magnetic, and/or electronic);[14] this has been realized in several f-electron compounds such as R$_x$Mo$_6$Se$_8$ (R=Tb,Er; x=1.0, 1.2),[15] $R_{1.2}$Mo$_6$S$_8$ (R=Tb,Dy,Er),[16] and ErRh$_4$B$_4$.[17] Recently, we reported TEM evidence for the

existence of an orthorhombic Ru-1212 phase with approximate unit cell parameters $\sqrt{2}a_t \times \sqrt{2}a_t \times 2c_t$ in a thin film.[18] A model of orthorhombic Ru-1212 with doubled c parameter, based on a periodic alternation of superconducting Ru$_{1-x}$Cu$_x$Sr$_2$GdCu$_2$O$_{8-\delta}$ layers and ferromagnetic RuSr$_2$GdCu$_2$O$_8$ layers, has been proposed. Also in bulk Ru-1212 an orthorhombic deformation has been detected and it has been attributed to a slight disorder and rotation of the RuO$_6$ octahedra around a, b, and c axes.[19]

Different studies of Ru-1212 have shown that the physical properties and the structural distortions strongly depend on the synthesis conditions. In particular, a high-temperature treatment (around 1060 °C) in flowing oxygen is necessary for the synthesis of a single-phase Ru-1212. On the other hand, it has been reported that Ru-1212 undergoes a solid phase decomposition close to the synthesis temperature ($\sim$1060 °C in oxygen and $\sim$1040 °C in air).[20] It was shown that physical properties of ruthenocuprate materials depend on the intragranular disorder of microdomains and defects in the bulk material.[21] In particular, a long-time annealing in flowing oxygen improves crystal perfection and properties as well.

Structure determination of superconducting and nonsuperconducting Ru-1212 in bulk and in thin-film form is mainly based on synchrotron x-ray powder diffraction[12,13,20] and neutron diffraction.[7] Up to now only a few TEM-based studies of the microstructure and defect structure of "Ru-1212"-type RuSr$_2\mathcal{R}$Cu$_2$O$_8$ ($\mathcal{R}$=Gd,Eu,Y) have been reported.[18,22–25] However, some of the data are contradictory and are a matter of discussion and/or interpretation. At the same time, it is absolutely clear that the local structure and, in particular, the homogeneity of the material may play a crucial role in the physical properties. We therefore investigated in detail the structure of single-phase bulk Ru-1212. The material unambiguously displays a Curie transition and bulk superconductivity.[22]
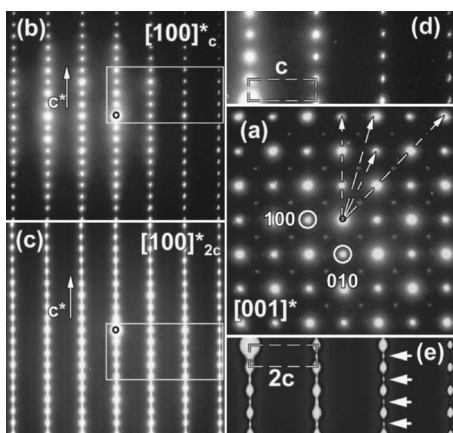
FIG. 1. Diffraction patterns of the Ru-1212 structure along two relevant zones: (a) $[001]^*$, (b), (c) $[100]^*$. (d), (e) are enlarged segments of the regions in rectangles in (b) and (c). The indexation is done with respect to the *P4/mmm* space group. Note the weak $(1/2)c^*$ superstructure spots marked by arrowheads in the enlargement (e).

The sample was first characterized by synchrotron x-ray diffraction and was found to have an average tetragonal structure.[25]

II. EXPERIMENT

Details of the synthesis procedure as well as of the synchrotron x-ray study are published elsewhere.[25] The $RuSr_2GdCu_2O_8$ sample was prepared by solid state reaction of RuO_2, $SrCO_3$, Gd_2O_3, and CuO powders. The powders were mixed, pelleted, and initially reacted at 1010 °C under flowing nitrogen to minimize the formation of $SrRuO_3$. The sample was then reacted under flowing oxygen at 1050, 1055, and 1060 °C, and slow cooled to room temperature. The product was phase pure by x-ray diffraction with all peaks indexed by a tetragonal *P4/mmm* cell [$a=3.82765(5)$, $c=11.5365(2)$ Å]. Resistivity measurements showed the sample to be superconducting with a T_c of 37 K. Thermogravometric analysis of the annealed sample gave an average stoichiometric oxygen content of 8.00 ± 0.02.

TEM investigations were made on crushed samples deposited on a holey carbon grid. High-resolution TEM (HRTEM) was carried out with a JEOL 4000EX microscope having a point resolution of 0.17 nm. Electron diffraction (ED) experiments were performed on a Philips CM20 microscope with a relatively high-angle tilting holder ($\pm45°$). High-angle annular dark-field (HAADF) scanning TEM (STEM) experiments were performed using a JEOL 3000F TEM/STEM electron microscope having a 0.2 nm STEM resolution. The MACTEMPAS CRYSTALKIT software was used for computer simulating the HREM and *Z*-contrast images.

III. RESULTS

A careful ED study of the bulk Ru-1212 sample revealed the coexistence of two closely related phases. Figure 1 shows a set of ED patterns taken along two relevant zone axes
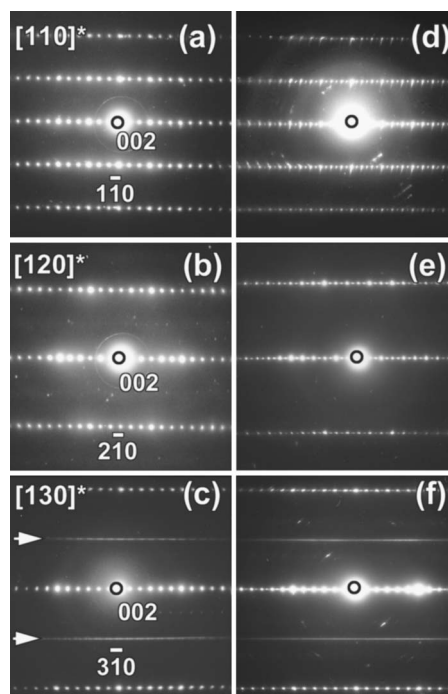

FIG. 2. ED tilting sequence around the c^* axis for both type structures: with normal *c* parameter (left) and with a 2*c* parameter (right).

$[001]^*$ and $[100]^*$. All major diffraction spots can be indexed with reference to the tetragonal *P4/mmm* space group, compatible with the synchrotron x-ray data.[22] However, weak additional reflections corresponding to a $\sqrt{2}a_t \times \sqrt{2}a_t$ superstructure are clearly visible in the $[001]^*$ ED pattern. These have been previously observed by several research groups in bulk.[22,8] as well as in thin-film materials[18] and attributed to a structure with *P4/mbm* symmetry and $\sqrt{2}a_t \times \sqrt{2}a_t \times c$ unit-cell parameters. Furthermore, on some of the ED patterns, viewed along $[100]^*$, weak superstructure reflections along the c^* direction are clearly visible [Figs. 1(c) and 1(e)]. It is also clear that the basic spots are elongated along the *c* direction and connected by streaks. The superstructure spots, indicated by arrows, are situated at $(0,0,l/2)$ and suggest a doubling of the *c* parameter. The streak pattern is a clear indication of planar disorder along the *c* axis whereas the doubling (2*c*) is related to an ordering of composition or tilting mode in one layer out of two. This doubling of the *c* parameter has been observed only in superconducting Ru-1212 epitaxial thin films[18] on a $SrTiO_3$ substrate, but never for bulk Ru-1212 either by x-ray (or neutron) diffraction or by electron microscopy.[22]

In order to clarify the relation between both phenomena, careful tilting experiments have been performed. Figure 2 shows two series of ED patterns taken from two crystallites along three identical zone axes $[110]^*$, $[120]^*$, and $[130]^*$ indicated by arrows in Fig. 1(a). All ED patterns for both phases exhibit identical features and the only difference is the doubling along the *c* direction in Figs. 2(d)–2(f). The $[110]^*$ and $[120]^*$ patterns can be indexed in both tetragonal space groups (SGs) (*P4/mmm* and *P4/mbm*) but the $[130]^*$ pattern unambiguously points to the *P4/mmm* structure. The
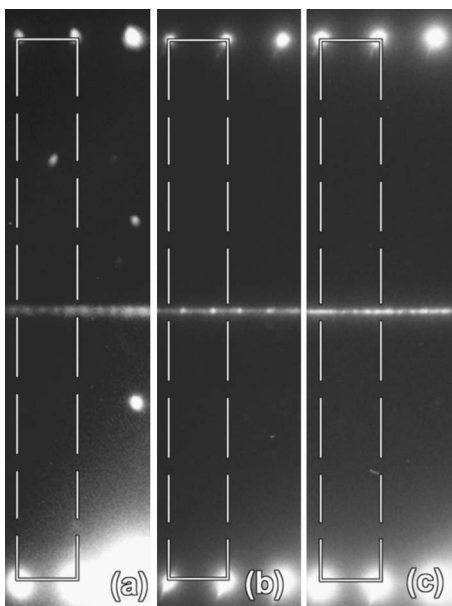
FIG. 3. Enlarged sectors of the $[1\bar{3}0]^*$ ED pattern with different $1/2\,\bar{3}1l$ superstructures along the c^* axis.

$(130)^*$ plane is passing through the superstructure spots [see Fig. 1(a)] and shows that, except for the row of $\frac{1}{2}\bar{3}1l$ spots, a row of diffuse intensity spots is present. This means that the weak superstructure spots in the $[001]^*$ pattern [Fig. 1(a)] actually result from the intersection of this diffuse row with the $[001]^*$ plane. An enlargement of the diffuse rows in the $[130]^*$ pattern [Fig. 3] shows that it is composed of a dense arrangement of weak superlattice reflections. The distance between these weak superlattice reflections varies from one crystal to another. For instance, the ED pattern in Fig. 3(a) shows a superlattice reflection separation of $(1/4)c^*$. Moreover these reflections are shifted over $(1/8)c^*$ with respect to the basic spots along $[001]^*$. The ED patterns in Figs. 3(b) and 3(c) exhibit a different superlattice d spacing. The presence of these superlattice reflections has been observed irrespective of the doubling of the c periodicity or of the streaking along c^*.

A HRTEM image of a highly crystalline and perfect Ru-1212 sample along $[100]$ is shown in Fig. 4. The image simulation based on the tetragonal $P4/mmm$ (127) structure[22] is given as an inset in Fig. 4 and shows that for this focus and thickness the brighter dots correspond to the light atoms and the darker dots represent the heavy atoms Ru and Gd.

A low-magnification TEM image of a disordered Ru-1212 crystal [see the corresponding ED pattern in Fig. 1(c)] is shown in Fig. 5. It shows the coexistence of order, disorder, and the basic Ru-1212 structure within one single crystal. The disordered area of a few hundred nanometers wide contains planar defects with a tendency to a double-c periodicity. Locally a tripling or a random configuration occurs. This observation of planar disorder is clearly related to the streaking and doubling in the corresponding ED pattern [Fig. 1(c)].

The doubling of the periodicity is highlighted in the $[100]$ HRTEM image of Fig. 6. The doubling of more intense bright dot layers along the c axis is apparently related to the
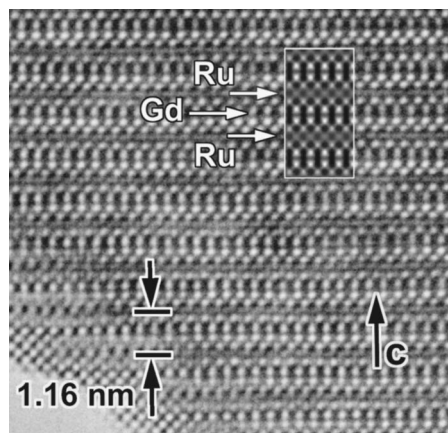

FIG. 4. HREM image of a perfect Ru-1212 crystal along $[100]$. The inset shows a simulated image based on the tetragonal $P4/mmm$ space group (defocus value $\Delta f=-60$ nm and thickness $t=4$ nm). The position of Ru and Gd cations is marked by white arrows.

fact that successive RuO_2 layers are no longer equivalent and they are imaged with a different contrast. Simulated images indeed allow us to identify that for this imaging condition the less bright contrast rows correspond to the RuO_2 layers whereas substitution of Ru by Cu leads to increasing brightness of the rows.

To determine the nature of these planar defects, we performed HAADF imaging in STEM mode. This so-called Z-contrast technique produces an incoherent image where the intensities are functions of the Z number of the elements. Therefore, the heavy-atom columns are imaged as the brighter dots. A major advantage of the Z-contrast technique is its lower sensitivity to small deviations from the exact zone axis orientation and the strongly reduced influence of dynamic effects like double diffraction. Conventional HR-TEM and high-resolution Z-contrast techniques are therefore
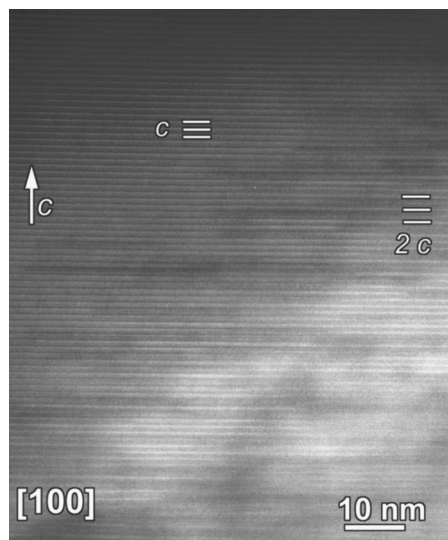

FIG. 5. $[100]$ low-magnification image showing disorder in the Ru-1212 crystal. Two regions can be clearly discerned: a perfect Ru-1212 structure with a repeat period c (upper part) and a disordered region with locally a $2c$ periodicity (middle and lower parts).
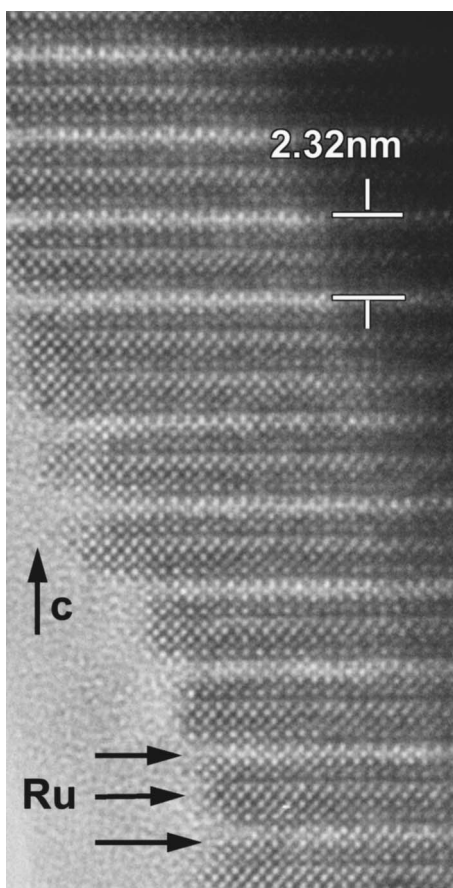
FIG. 6. [100] HREM image of Ru-1212 with $2c$ parameter.

highly complementary and provide extra structural and chemical information. A [100] Z-contrast image of a disordered region is shown in Fig. 7. The low-magnification image clearly shows the same kind of planar defects as in Fig. 5, randomly distributed within the crystal. The defects are characterized by a darker contrast with respect to the normal structure, i.e., lighter elements have to be present in
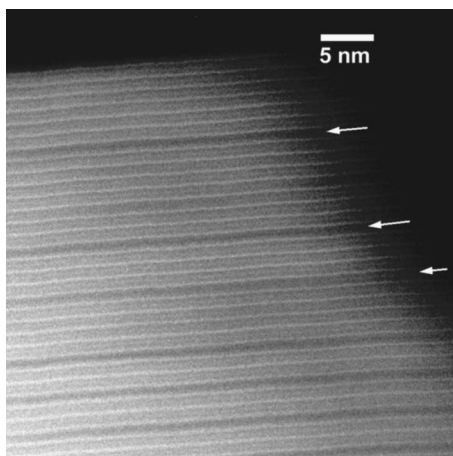

FIG. 7. Low-magnification HAADF image along [100] of a defect structure. The brighter lines correspond to the Gd layer whereas the less bright ones are the Ru layers. Note the clear dark lines at the position of the Ru layers marked by white arrows.
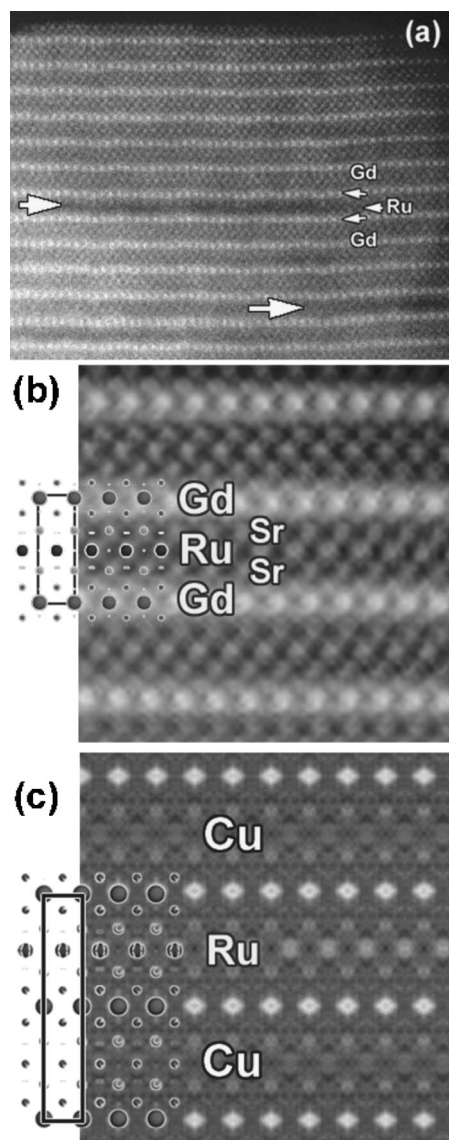

FIG. 8. (a) High-resolution [100] Z-contrast image of Ru-1212. The defect layer exhibits a depletion of intensity at the position of the Ru layer. (b) Enlarged image with an overlay of the Ru-1212 structure model. (c) Z-contrast simulated image for full Cu substitution in the RuO_2 layer. Note the decrease of intensity due to the Cu substitution.

this layer. A high-resolution Z-contrast image of the Ru-1212 structure is shown in Fig. 8. The brighter dots can be associated with the heavier Gd ($Z=64$) layers and the less bright dots correspond to the position of the Ru ($Z=44$) layers, located exactly between two Gd layers. The four Sr ($Z=38$) positions are imaged as weaker dots in a square arrangement around the Gd position [Fig. 8(b)]. The most likely substitution is a Cu substitution in the Ru layer, giving rise to a $(Ru_{1-x}Cu_x)$ composition in this layer. A HREM Z-contrast simulated image based on a simple substitution of Ru by Cu is represented in Fig. 8(c) and shows a good qualitative correspondence with the experimental image.

Apart from the defect structure along the c axis, the material also contains other defects, such as 90° rotation do-
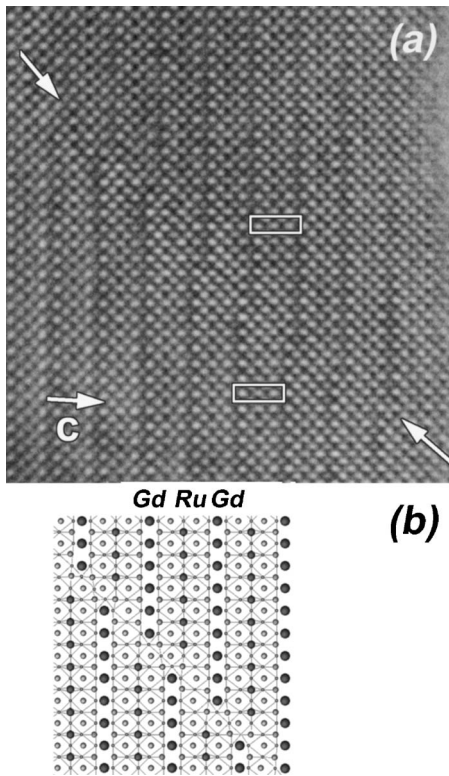
Gd Ru Gd

FIG. 9. (a) [100] HREM image of a (130) antiphase boundary; the projected unit cell has been indicated on both sides of the boundary (marked by arrows). (b) Structural model of a (130) antiphase boundary, taking into account all experimental evidence.

mains, antiphase boundaries (APBs) and dislocations. The 90° domains are the result of the three possible orientations of the c axis and are typical for tetragonal structures. APBs with a displacement vector $\mathbf{R}=[0\ 0\ 1/3]$ are frequently observed in thin films as a result of nucleation at a substrate step, but they were only occasionally observed in bulk material. A HRTEM image of an APB in Ru-1212 is shown in Fig. 9. The lattice planes of the cations are shifted with respect to each other over $\mathbf{R}=[0\ 0\ 1/3]$.

The APB boundary plane is always (130) and shows a good coherence across the boundary. The square bright dot pattern in Fig. 9, produced by the cation columns, is perfectly continuous across the boundary. This means that the perovskite-based lattice is continuous across the APB. However, there is a significant size difference between the successive layers in the perfect Ru-1212 structure ($d_{Gd-Sr}=0.357$ nm; $d_{Sr-Sr}=0.443$ nm; $d_{Ru-Cu}=0.411$ nm; $d_{Cu-Cu}=0.335$ nm) inducing a strain field along the APB. The mismatch along the boundary implies the presence of a locally distorted structure with a somewhat different atomic bonding or cation rearrangement. A model is shown in Fig. 9(b). The boundary is formed by vertex-sharing RuO_6 and distorted CuO_6 octahedra, leading to a local change in Cu-Ru stoichiometry. The difference in ionic size and atomic bonding of Ru and Cu allowed us to play with various stacking combinations that partially release the local strain at the boundary. However, numerous amounts of dislocations have been found at the boundary. Figure 10 shows a HREM image
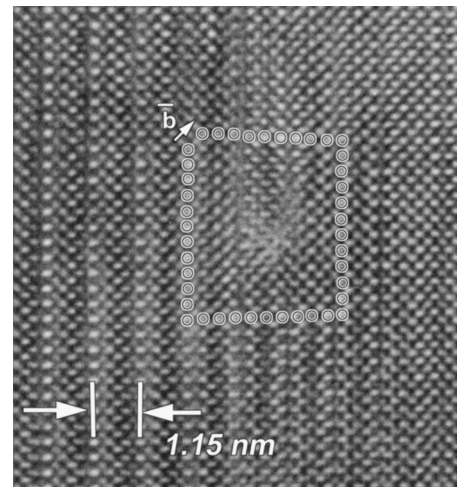

FIG. 10. HREM image of a partial dislocation at the APB. An associated Burgers circuit is indicated.

of such a dislocation surrounded by a Burgers circuit. The projection of the Burgers vector has a length $\approx\sqrt{2}a_p$ and a direction along [130]. These defects, however, have only very local and very small influence on the overall stoichiometry.

IV. DISCUSSION

A. Structure of $RuSr_2GdCu_2O_8$

The first question to be settled is that of the crystal structure of the basic Ru-1212 phase. Two structures of Ru-1212 have been reported, one determined by synchrotron x-ray diffraction[22] and another by neutron powder diffraction investigation.[24] The first one is tetragonal with space group *P4/mmm* (*123*) and lattice parameters $a=0.383\ 84$ nm, $c=1.1573$ nm,[22] and structurally related to $YBa_2Cu_3O_{7-x}$ with Y, Ba, and Cu(1) being replaced by Gd, Sr, and Ru, respectively. It contains corner-sharing RuO_6 octahedra substituting for the Cu-O chains. The Ru atoms reside in the octahedra and are surrounded by six oxygen atoms: four equatorial atoms (O1) and two apical ones (O4). Chmaissem *et al.*[8] reported neutron powder diffraction data for $RuSr_2GdCu_2O_8$ where weak superlattice reflections indicated a $\sqrt{2}a_p\times\sqrt{2}a_p\times c$ cell as a result of the RuO_6 octahedra rotation around the c axis. The model is described by a tetragonal space group *P4/mbm* (*127*) (*0kl, k=2n; h00, h=2n*) with unit-cell parameters $a=0.542\ 49$ nm, $c=1.156\ 28$ nm. However, none of these space groups completely satisfies the extinction conditions found by electron diffraction. In particular, the presence of the $\sqrt{2}a_p\times\sqrt{2}a_p$ superstructure spots in the $[001]^*$ ED pattern [Fig. 1(a)] and the extinction condition *0k0, h00, h,k=2n*, are in contradiction with the model based on a *P4/mmm* space group; on the other hand the absence of *hkl, h=2n*, reflections in the $[120]^*$ zone contradicts the *P4/mbm* structure, although the intense diffuse streaks along c^* are situated at the position of the *hkl, h=2n* spots. Yokosawa *et al.* recently proposed a model explaining the appearance of the streaks based on the coexistence of nanometer-size domains of a primitive and a body-centered
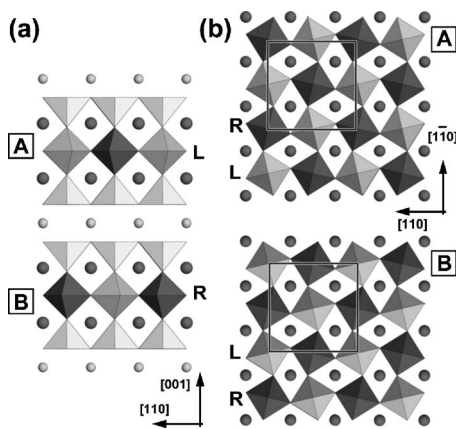
FIG. 11. (a) Schematic representation of the Ru-1212 structure viewed along [100] with different *nAmB* stacking along the *c* axis. The different sense of the RuO$_6$ octahedra rotation is denoted as *L* (left handed) and *R* (right handed). (b) [001] view of the two possible RuO$_2$ layers (*A* and *B*) dependent on the RuO$_6$ rotation.

tetragonal structure (*P4/mbm* and *I4/mcm*) along the *c* axis.[25] Thus in the case of the *P4/mbm* structure, reported in [22], only the *21l* and *21 l/2* diffraction spots should be present in the streaked row of the [120]* ED pattern separated by $(1/2)c^*$. Obviously, this is not the case. Moreover, the possible *21l* and *21 l/2* spots are mostly absent or have a minimum intensity. The basic spots on the most relevant ED patterns (see Fig. 1) are still consistent with both proposed tetragonal structures and only the streaks along the *c** direction in the [130]* ED pattern violate the extinction conditions. The streaking in the ED as well as the HREM results point toward a stacking disorder of the layers along the *c* direction, but maintaining the basic Ru-1212 structure. The appearance of the $\sqrt{2}a_p \times \sqrt{2}a_p$ superstructure spots in the [001]* ED pattern strongly suggests a rotation of the RuO$_6$ octahedra in the (001) plane,[22,8] as shown schematically in Fig. 11. The octahedra are rotated around the *c* axis in opposite senses, i.e., two neighboring octahedra are left- (*L*) and right-hand (*R*) rotated. The suggested *P4/mbm* SG with $\sqrt{2}a_p \times \sqrt{2}a_p \times c$ parameters requires the same sense of rotation along the *c* axis (*L-L-*··· or *R-R-*···). However, a shift of one RuO$_6$ layer with respect to the next one along the [100] direction with a displacement vector $R = a_p$ leads to a mixing in the sense of rotation as well (*L-R-*···). In this case, two different layers of RuO$_6$ octahedra (denoted as *A* and *B* in Fig. 11) can occur along the *c* axis. It should be noted that this shift does not affect the basic structure and the position of all cations remains unaltered. Finally, the structure of Ru-1212 could be expressed in terms of a stacking of RuO$_6$ layers as follows: *nAmB*, where *n* and *m* are integers, indicating the number of *A* and *B* layers in the sequence. The resulting ED patterns (Fig. 2) are then a superposition of the patterns from the different stacking sequences.

Long stacking sequences are best observed at low magnification in the dark-field mode and in the thicker parts of the crystal, as shown in Fig. 12. The alternating disorder of the RuO$_6$ layers is clearly visible in dark-field images selecting the superlattice reflection row in the objective aperture (marked by a white circle in the ED pattern of Fig. 12).
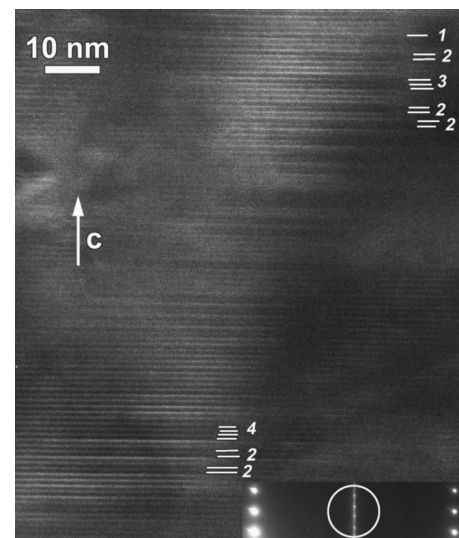

FIG. 12. Dark-field TEM image obtained by exciting the superlattice reflections marked in the inset ED pattern by a white circle.

Different superperiods (*2A3B*, *3A4B*,…) are imaged as a sequence of dark and bright lines corresponding to *A*- or *B*-type layers. The superposition of different types of superstructures randomly distributed within the crystal produces streaks in the [130]* pattern. Therefore, our observations suggest that the Ru-1212 structure contains different combinations of *nA* or *mB* lamella where $n, m = 0, 1, 2, \dots$. In this respect, the body-centered tetragonal structure proposed by Yokosawa *et al.*[24] is a special case of the general formula and can be described as *AB* ($n = m = 1$). The ED patterns of the superstructures in Fig. 3 can be described as *2A3B* [Figs. 3(a) and 3(b)] *3A4B*.

B. Structure of (Ru$_{1-x}$Cu$_x$)Sr$_2$GdCu$_2$O$_8$

Based on our EM results, combining HREM and ED patterns, we can conclude that the so-called Ru-1212 is often better described as (Ru$_{1-x}$Cu$_x$)-1212; the structure of (Ru$_{1-x}$Cu$_x$)-1212 being close to that of Ru-1212. ED reveals similar extinction conditions and a difference only occurs in the RuO$_6$ octahedral layers resulting in a doubling of the *c* parameter. Our TEM and STEM results provide unambiguous evidence of the substitution of Ru by a lighter element. HRTEM images (Fig. 6) exhibit a brighter contrast at the Ru defect layer and also *Z*-contrast images (Figs. 7 and 8) show that the defect Ru layers are less electron dense. The most likely origin is a Cu substitution for Ru, producing an (Ru$_{1-x}$Cu$_x$)-1212 phase. The simulated *Z*-contrast [Fig. 8(c)] and HREM images (Fig. 6) demonstrate a good agreement with the experiment when substituting Cu for Ru in the Ru layer. These "defect" layers are often randomly distributed within the crystal (Figs. 5 and 7), but over relatively large areas there is a tendency to occur every second layer; i.e., a doubling of the *c* parameter. The corresponding ED patterns [Figs. 1(c) and 2] then exhibit a sharp extra reflection at $(1/2)[001]^*$. Because of this tendency of alternating Ru and (Ru-Cu) layers it is reasonable to consider a different "Ru-1212" structure with a doubled *c* parameter. This dou-

bling of the c parameter in Ru-1212, related to an ortho-rhombic distortion, has recently been reported in thin films.[17] Indeed for thin films, the epitaxial stress and the imposed substrate orientation can induce an orthorhombic distortion. A careful analysis of $[001]^*$ ED patterns in the present case did not reveal any distortion of tetragonal symmetry. Hence, the unit-cell parameters of the $(Ru_{1-x}Cu_x)Sr_2GdCu_2O_8$ phase may be written as $a_s=b_s=\sqrt{2}a_T$, $c_s=2c_T$, where a_T and c_T are the unit-cell parameters of the *P4/mmm* structure. It should be noticed that no difference in d spacing between c_T and $c_s/2$ has been found. This means that there is no significant expansion along the c axis due to the Cu substitution. At the same time, it was found that the c/a axis ratio varied between 3.03 and 3.05. This value is slightly higher than that found from synchrotron x-ray data.[21] One of the most difficult and intriguing points is the structure of the substituted layer. Since none of the techniques are able to provide a direct and unambiguous answer, we will combine all information available from TEM, STEM, and ED results. An important, but difficult question is the level of the Cu substitution in the (Ru-Cu) layer. Directly measuring the exact Cu content in a single layer is nearly impossible through direct methods such as electron energy-less spectroscopy, but the set of simulated HRTEM and Z-contrast images for different levels of Cu substitution allow us to make some reasonable predictions. The best fit between the calculated and experimental HR-TEM and Z-contrast images is achieved for a complete Cu substitution [Figs. 6 and 8(c)]. This would mean that the Ru-1212 with the doubled c axis can be described as a succession of $CuO_{2-\delta}$-RuO_6 layers and the final formula could then be written as $RuSr_4Gd_2Cu_3O_{15-\delta}$. The second question concerns the structure of the Ru and Cu layers. Whenever the $\sqrt{2}a_p \times \sqrt{2}a_p$ superstructure spots appear in the $[001]^*$ ED (and corresponding superstructure spots in the $[130]^*$ pattern) together with a doubling of the c parameter, the pure RuO_6 layer will maintain its structure from the Ru-1212 basic *P4/mbm* structure. The presence of streaks in the $[130]^*$ pattern definitely points toward an ordering in the rotation of the RuO_6 octahedra. However, the superstructure ordering is more complex because of the occurrence of Cu-O layers. How will a Cu substitution affect the RuO_6 octahedral layer? An extra problem is that Cu can accept different coordination environments. It is therefore difficult to exclude that Ru substitution by Cu will lead to an oxygen rearrangement around the Ru (Cu) site and create, for instance, Cu chains instead of RuO_2 planes (Fig. 13). The lengths of the Cu-O bonds in plane and the Ru-O bonds are very close [1.94 Å for Cu-O (Ref. 26) and 1.96 Å equatorial and 1.93 Å apical for Ru -O (Ref. 22)] which means that no significant distortions or changes in unit-cell parameter should occur. The replacement of a RuO_2 square planar layer by CuO chains should induce an orthorhombic distortion in the Ru-1212 structure[17] similar to that in $YBa_2Cu_3O_{7-x}$. However, we did not observe any evidence of an orthorhombic distortion in either ED or HREM. On the other hand, we did observe a tetragonal structure in $YSr_2Cu_3O_{6+x}$[27] having CuO chains. The proposed model in that case is based on a sequence of CuO_2 planes rotated 90° around the c axis and implies an oxygen deficiency in agreement with the synchrotron and neutron
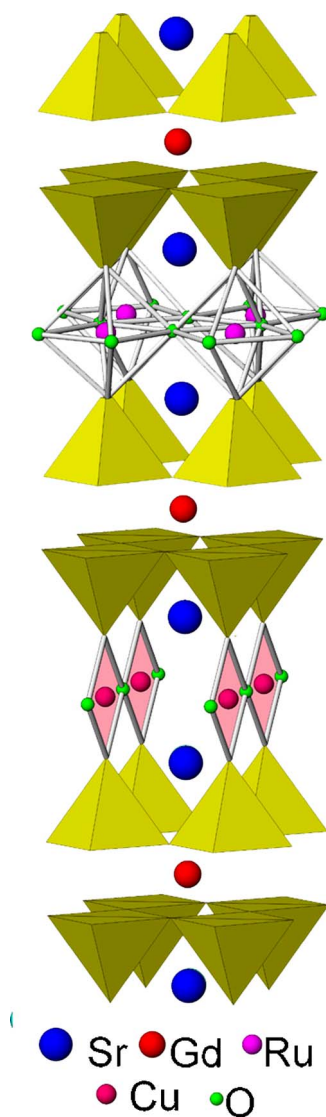

FIG. 13. (Color online) Schematic representation of the $Ru_{1-x}Cu_xSr_2GdCu_2O_{8-\alpha}$ structure.

diffraction data. Another possibility is that Cu directly substitutes Ru in the RuO_6 octahedra without oxygen rearrangement. But in this case, we would have Cu^{2+}, octahedrally surrounding by six oxygen atoms, and a Jahn-Teller distortion should occur. The apical and equatorial Cu-O distances for different types of Jahn-Teller distorted octahedra are 1.786 and 1.929 Å for $YBa_2Cu_3O_{6.35}$,[28] or 1.79, 1.934, and 1.926 Å for $Y_2Ba_4Cu_7O_{14.30}$.[29] Apparently, the difference between Ru-O and Cu-O bond lengths is much bigger than that in the CuO_2 plane and Cu substitution will require a strong distortion of the structure. As a consequence, the unit-cell parameters should change significantly. For example, the shorter apical distance (1.78 Å for Cu-O and 1.92 Å for Ru-O) should result in a decrease of the c parameter. Obviously, this is not the case for the $(Ru_{1-x}Cu_x)$-1212 phase because no changes in c parameter have been found. Other coordination environments for Cu, such as pyramids or dumbbells, seem to be very unlikely for the Ru-1212-type structure. Taking into account all these structural consider-

ations and experimental data, we propose the following structural model for the $(Ru_{1-x}Cu_x)$-1212 phase, schematically shown in Fig. 13. $(Ru_{1-x}Cu_x)$-1212 has a structure similar to that of Ru-1212 where the unit cell has been enlarged to $\sqrt{2}a_p \times \sqrt{2}a_p \times 2c$ as a result of rotations of the RuO_6 octahedra and Cu substitution in one Ru layer out of two. The sense of rotation is completely ordered along the c axis resulting in different stacking sequences. The Cu-substituted layer most probably consists of CuO_2 planes instead of RuO_6 octahedra leading to an oxygen deficiency. The effect of heterovalent substitution in ruthenocuprates on the physical properties has been reported recently by Klamut *et al.*[13,30] A heterovalent doping has been achieved through partial substitution of Cu ions into the RuO_2 planes ($0 \leq x \leq 0.75$) at high-pressure oxygen conditions and with Ce ions into the Gd sites. It was found that T_c increases with the Cu content and reaches a maximum ($T_c^{max}=72$ K) for $x=0.3-0.4$. A further increase of x makes T_c drop again ($T_c=62$ K for $x=0.75$). No data are available for higher x values. However, taking into account the $T_c(x)$ behavior and oxygen deficiency in $RuSr_4Gd_2Cu_3O_{15-\delta}$ it is plausible that the (minority) phase has a T_c close to the measured ($T_c=37$ K). This makes it possible that actually the $RuSr_4Gd_2Cu_3O_{15-\delta}$ structure is responsible for superconductivity and opens the discussion of the homogeneity of the material.

phase is not homogeneous and contains two distinct but closely related structures: $RuSr_2GdCu_2O_8$ and $RuSr_4Gd_2Cu_3O_{15-\delta}$. The first phase, with unit-cell parameters $\sqrt{2}a_p \times \sqrt{2}a_p \times c$, exhibits ordering along the [100] direction because of rotated RuO_6 octahedra and can be expressed in terms of stacking RuO_6 lamella layers each shifted with respect to the next one over a vector $R=a_p$. The $RuSr_4Gd_2Cu_3O_{15-\delta}$ structure can be described as a periodic alteration along the c axis of CuO_4 planes and RuO_6 octahedra. The unit-cell parameters of this phase are $\sqrt{2}a_p \times \sqrt{2}a_p \times 2c$. The possible influence of this phase and its defect structure on the sensitivity of the superconductivity and magnetic properties is discussed.

The Cu doping is important for understanding the relation and coexistence of magnetism and superconductivity in Ru-1212. The Cu substitution in the RuO_2 layer could be responsible for superconductivity instead of (or as well as) the Ru-Cu band overlap. If we assume Cu^{2+} substituting for Ru^{5+}, then x would only need to be 0.05 to give the measured $7-8$ % hole-doping superconductivity. Obviously, such levels of Cu doping would not affect very much the long-range ferromagnetism of Ru. Our results do not suggest that superconductivity and magnetism are macroscopically separated phases, but could suggest that superconductivity is related to the Cu-substituted regions.

V. CONCLUSIONS

The structure and defect structure of "perfect" bulk superconducting ferromagnetic $RuSr_2GdCu_2O_8$ has been investigated. It has been shown that on a local scale the Ru-1212

ACKNOWLEDGMENTS

*Author to whom correspondence should be addressed.

[1] J. D. Jorgensen, D. G. Hinks, P. G. Radaelli, Pri Shiyou, P. Lightfoot, B. Dabrowski, C. U. Segre, and B. A. Hunter, Physica C **185-89**, 184 (1991).

[2] O. Chmaissen, P. Guptasarma, U. Welp, D. G. Hinks, and J. D. Jorgensen, Physica C **292**, 305 (1997).

[3] H. W. Zandbergen, R. Gronsky, K. Wang, and G. Thomas, Nature (London) **331**, 596 (1988).

[4] J. Karpinski, E. Kaldis, E. Jilek, S. Rusiecki, and B. Bucher, Nature (London) **336**, 660 (1988).

[5] G. Van Tendeloo, C. Chaillout, J. J. Capponi, M. Marezio, and E. V. Antipov, Physica C **223**, 219 (1994).

[6] J. L. Tallon, C. Bernhard, M. E. Bowden, P. M. Gilberd, T. M. Stoto, and D. J. Pringle, IEEE Trans. Appl. Supercond. **9**, 1696 (1999).

[7] J. D. Jorgensen, O. Chmaissem, H. Shaked, S. Short, P. W. Klamut, B. Dabrowski, and J. L. Tallon, Phys. Rev. B **63**, 054440 (2001).

[8] O. Chmaissem, J. D. Jorgensen, H. Shaked, P. Dollar, and J. L. Tallon, Phys. Rev. B **61**, 6401 (2000).

[9] V. L. Ginzburg, Sov. Phys. JETP **4**, 153 (1957).

[10] C. Bernhard, J. L. Tallon, C. Niedermayer, T. Blasius, A. Golnik, E. Brhcher, R. K. Kremer, D. R. Noakes, C. E. Stronach, and E. J. Ansaldo, Phys. Rev. B **59**, 14099 (1999).

[11] W. E. Pickett, R. Weht, and A. B. Shick, Phys. Rev. Lett. **83**, 3713 (1999).

[12] A. C. McLaughlin and J. P. Attfield, Phys. Rev. B **60**, 14605 (1999).

[13] P. W. Klamut, B. Dabrowski, S. Kolesnik, M. Maxwell, and J. Mais, Phys. Rev. B **63**, 224512 (2001).

[14] P. W. Anderson and H. Suhl, Phys. Rev. **116**, 898 (1959).

[15] R. W. McCallum, D. C. Johnston, R. N. Shelton, W. A. Fertig, and M. B. Maple, Solid State Commun. **24**, 501 (1977).

[16] M. Ishikawa and Ø. Fisher, Solid State Commun. **24**, 747 (1977).

[17] W. A. Fertig, D. C. Johnston, L. E. DeLong, R. W. McCallum, M. B. Maple, and B. T. Matthias, Phys. Rev. Lett. **38**, 987 (1977).

[18] O. I. Lebedev, G. Van Tendeloo, G. Cristiani, H.-U. Habermeier, and A. T. Matveev, Phys. Rev. B **71**, 134523 (2005).

[19] A. Martinelli, C. Artini, M. R. Cimberle, G. A. Costa, M. Ferretti, R. Masini, and P. Mele, Phys. Rev. B **69**, 052507 (2004).

[20] M. R. Cimberle, M. Tropeano, M. Ferretti, A. Martinelli, C. Artini, and G. A. Costa, Semicond. Sci. Technol. **18**, 454 (2005).

[21] A. T. Matveev, A. N. Maljuk, A. Kulakov, C. T. Lin, and H.-U. Habermeier, Physica C **407**, 139 (2004).

[22] A. C. McLaughlin, W. Zhou, J. P. Attfield, A. N. Fitch, and J. L. Tallon, Phys. Rev. B **60**, 7512 (1999).

[23] A. L. Vasiliev, M. Aindow, Z. H. Han, J. I. Budnick, W. A. Hines, P. W. Klamut, M. Maxwell, and B. Dabrowski, Appl. Phys. Lett.

85, 3217 (2004).

[24] T. Yokosawa, V. P. S. Awana, K. Kimoto, E. Takayama-Muromachi, M. Karppinen, H. Yamauchi, and Y. Matsui, Ultramicroscopy **98**, 283 (2004).

[25] A. C. Mclaughlin, V. Janowitz, J. A. McAllister, and J. P. Attfield, J. Mater. Chem. **11**, 173 (2001).

[26] P. Bordet, C. Chaillout, J. J. Capponi, J. J. Chenavas, and M. Marezio, Nature (London) **327**, 687 (1987).

[27] O. I. Lebedev, G. VanTendeloo, F. Licci, E. Gilioli, A. Gauzzi, A. Prodi, and M. Marezio, Phys. Rev. B **66**, 132510 (2002).

[28] R. J. Cava, A. W. Hewat, E. A. Hewat, B. Batlogg, M. Marezio, K. M. Rabe, J. J. Krajevski, W. F. Peck, and L. W. Rupp, Physica C **165**, 419 (1990).

[29] P. Bordet, C. Chaillout, J. J. Chenavas, J. L. Hodeau, M. Marezio, J. Karpinski, and E. Kaldis, Nature (London) **334**, 596 (1988).

[30] P. W. Klamut *et al.*, J. Appl. Phys. **91**, 7134 (2002).